Antibacterial effectiveness meets improved mechanical properties: natural hydrogels based on Manuka Honey and Gellan Gum for cartilage regeneration

Maria A. Bonifacio[a], Stefania Cometa[b], Andrea Cochis[c], Piergiorgio Gentile[d], Ana M. Ferreira[d], Barbara Azzimonti[c,g], Giuseppe Procino[e], Edmondo Ceci[f], Lia Rimondini[c,g§], Elvira De Giglio [a§*]

[a] Department of Chemistry, University of Bari "Aldo Moro", Italy
[b] Jaber Innovation s.r.l., Italy
[c] Department of Health Sciences, University of Piemonte Orientale "UPO", Italy
[d] School of Engineering, Newcastle University, UK
[e] Department of Veterinary Medicine, University of Bari "Aldo Moro", Italy
[f] Department of Biosciences, Biotechnologies and Biopharmaceutics, University of Bari "Aldo Moro", Italy
[g] INSTM, Consorzio Interuniversitario Nazionale per la Scienza e Tecnologia dei Materiali, Firenze, Italy.
[§] co-shared authorship

Corresponding author e-mail: elvira.degiglio@uniba.it*

Abstract

Biomaterials for cartilage repair are still far from clinical requirements, even if several studies recently focused on this topic. In this respect, Nature-derived hydrogels are a promising class of scaffolds for cartilage tissue engineering, mimicking the native cellular microenvironment. However, they frequently lack mechanical fea- tures required for cartilage applications and are commonly subjected to infection threat. This work describes the innovative use of Manuka honey as molecular spacer for preparing gellan gum-based composites with intrinsic antibacterial properties and superior compressive Young's modulus in respect of several Nature-derived gels based on chitosan, hyaluronic acid or alginate. The addition of Manuka honey made hydrogels able to inhibit the proliferation of S. aureus and S. epidermidis clinical isolates. Furthermore, no cytotoxic effects were detected on human mesenchymal stem cells seeded on the hydrogels. Moreover, chondrogenesis experiments showed a consistent expression of collagen II and high synthesis of GAGs and proteoglycans, thus indicating the formation of cartilage matrix. Overall, these data

suggest that the developed smart composites have a great potential as tools for cartilage tissue engineering.

Keywords: Manuka honey, Gellan gum, Hydrogel characterisation, Mechanical properties, Antibacterial, Cartilage regeneration.

1. Introduction

Since 1960s, hydrogels are among the most attracting polymeric materials for tissue engineering, thanks to their high water content and nutrients diffusion, making them ideal candidates as scaffolds for cell colonization and differentiation (Caló & Khutoryanskiy, 2015).

These features are particularly useful for cartilage tissue en- gineering, since a proper substitute is required to compensate the lim- ited self-healing potential of cartilage (Zhang, Zhang, & Yang, 2017). Hydrogels for cartilage repair are obtained from natural and synthetic biomaterials. Among Nature-derived hydrogels, polysaccharide-based ones (e.g. based on gellan gum, alginate and chitosan) are particularly interesting because of their low immunogenic profile, easy handling and low costs (Leone & Barbucci, 2009). Nature-derived hydrogels are more biocompatible as compared to synthetic hydrogels, although their mechanical features still need to be improved (Zhu & Marchant, 2011). To overcome this drawback, several studies describe the functionali- zation of these polymers with chemical moieties, exploited to support the hydrogel crosslinking (Liu et al., 2017). This approach leads to a moderate improvement of compressive Young's modulus (e.g. up to 10–50 kPa), still far from the mechanical requirements of cartilagineous tissue (Palumbo et al., 2015). Therefore, the preparation of composite hydrogels is currently being explored and represents one of the most promising available strategies (Yang, Zhang, Yue, & Khademhosseini, 2017). In this respect, gellan gum-based composite hydrogels (e.g., blends of gellan gum and polyvinyl

alcohol or gelatin) show interesting mechanical properties and bio-printability (Mouser et al., 2016; Wang, Wen, & Bai, 2016). In addition, Nature-derived hydrogels have to face the worrying issue of contamination, which could have a dramatic clinical outcome. Indeed, even if surgery-related infections of cartilagineous tissue are uncommon (Stutz, Kuster, Kleinstück, & Gächter, 2000), they could cause severe complications (i.e. septic arthritis) mainly due to Staphy- lococci (Wyatt, Maletis, Lyon, Schwalbe, & Avins, 2017). The inclusion of antimicrobials into the hydrogel networks is the traditional method to prevent contamination. Recently, the development of hydrogels with intrinsic antimicrobial activity has emerged as an effective alternative. Indeed, hydrogels based on antimicrobial peptides or cationic biopo- lymers (e.g. chitosan, polycarbonate containing quaternary ammonium groups) actively inhibit bacterial proliferation (Anjum, 2016; Liu et al., 2012).

In this scenario, the present work follows a Nature-inspired strategy, using Manuka honey to test two main hypotheses: 1) the exploitation of Manuka honey and its unique viscosity to enhance hydrogels' me- chanical features 2) the potential to overcome simultaneously con- tamination risks. Recently, the New Zealand Manuka honey (MH), derived from Leptospermum scoparium, is very attractive because of the remarkable non-peroxide antibacterial activity of methylglyoxal (MGO, or Unique Manuka Factor). Since 2015, when Manuka honey was defined "a tissue engineering essential ingredient" (Speer, Schreyack, & Bowlin, 2015), it was employed as diet supplement or wound dresser in combination with chitosan (Carter et al., 2016; Sasikala & Durai, 2015). However, at the best of our knowledge, the neat Manuka honey has never been exploited to synthesise implantable hydrogels. In this work, considering the high viscosity of MH, it was added, for the first time, as molecular spacer to prepare an innovative gellan gum- based implantable hydrogel for cartilage tissue engineering. The pre- sent work explores the intrinsic antibacterial properties of the prepared hydrogels, as well as the improvements in mechanical features. A fur- ther enhancement of

hydrogels compressive Young's modulus was also achieved by suitable crosslinkers, such as the cations Mg2+ and Ca2+, alone or in combination with the natural Halloysite nanotubes (HNT), added as inorganic filler. Since the percentage of the latter is re- sponsible for the hydrogels compressive strength, the HNT amount was properly chosen to maximise mechanical performances as previously reported (Bonifacio, Gentile, Ferreira, Cometa, & De Giglio, 2017).

The characterisation of the prepared hydrogels was achieved by X- ray Photoelectron Spectroscopy (XPS) and porosity measurements, while the mechanical performances were extensively investigated through compression and stress-relaxation studies. The in vitro anti- bacterial effectiveness of the hydrogels was studied against clinical multi drug resistant (MDR) isolates of S.aureus and S.epidermidis, se- lected for their pivotal role in cartilage infections. Finally, cyto-compatibility was evaluated on human mesenchymal stem cells (hMSCs), successfully induced to differentiate into chondrocytes on the hydrogels surfaces. The reported results showed a great potential of the prepared hydrogels for cartilage repair.

2. Materials and methods

2.1. Materials

Unless otherwise specified, all reagents were supplied by Sigma- Aldrich (Italy). Gellan gum, hereafter named GG (PhytagelTM, formula weight 1,000Kg/mol, low acylation degree) was a linear anionic poly- saccharide, consisting in the repetition of a tetrasaccharide unit, β-D- glucose-β-D-glucuronic acid-β-D-glucose-α-L-rhamnose, in a 2:1:1 ratio. Halloysite nanotubes ($Al_2Si_2O_5(OH)_4 \cdot 2H_2O$) had a mean diameter of 30–70 nm and a mean length of 1–3 μm. $CaCl_2$ and $MgCl_2$ salts are of Redi-driTM grade. Medical grade Manuka honey12Plus (MH) (ManukaGuard®, US) contained 400 mg/Kg of MGO. Ultrapure water was obtained by a Milli-Q® Integral system (Millipore-Merck, Italy). The TRI Reagent® and all the media/supplements for isolation and culture

of bacteria and human cells were from SigmaAldrich, while the XTT assay was from LifeTechnologies (Italy). The hanging tissue culture inserts for 24-well plates were from Sarstedt (Italy). The 24-well plates used with the NunclonTM Delta Surface treatment, were supplied by ThermoFisher Scientific (Italy), as well as the 96-well plates. The TaqMan reverse transcription kit was from AppliedBiosystems (Italy).

2.2. Hydrogels preparation

Hydrogels were obtained as previously reported (Bonifacio et al., 2017) for GG-based hydrogels containing glycerol as molecular spacer. Briefly, GG powder (2%w/v) was dissolved under stirring in 100 mL of water at 90 ± 0.5 °C, using an ARE Aluminium hot plate stirrer (VELP Scientifica, Italy). After cooling the solution at 60 ± 0.5 °C, MH (2%w/ v) was added and vigorously stirred. HNT-reinforced samples were obtained mixing the dissolved components with an aqueous suspension of HNT (0.5 w/v), previously sonicated in water for 15 min. To obtain mechanical stability of the prepared hydrogels, a crosslinking was achieved through the external gelation method (Kaklamani, Cheneler, Grover, Adams, & Bowen, 2014) using as cationic sources CaCl2 or MgCl2 solutions under physiological concentrations (0.025%w/v and 0.5%w/v respectively). A list of the hydrogels types prepared in this work is reported in Table 1.

2.3. Spectroscopic characterisation

Spectroscopic characterisation of the hydrogels was carried out by X-ray Photoelectron Spectroscopy (XPS). Hydrated samples were frozen for 24h at -20 ± 0.1°C, then freeze-dried at -55 ± 3°C for 48h with an ALPHA1-2/LDPlus (Martin-Christ, Germany). Thus, dried hydrogels were examined by a scanning microprobe PHI5000VersaProbeII (Physical Electronics, US), equipped with a monochromatised AlKα X- ray radiation source. The base pressure in analysis chamber was 10−9 mbar. Samples were analysed in High Power mode with an X-ray take- off angle of 45° (scanned size∼1400 × 200 μm). For each specimen, survey scans (Fixed Analyser Transmission mode, binding

energy (BE) range 0–1200eV, pass energy 117.4eV) and high-resolution spectra (FAT mode, pass energy 29.35 eV) were acquired. Data analysis was performed using the MultiPak software package (version9.6.1.7). Charge referencing was carried out setting the lower binding energy C1s photo-peak (i.e., C1s hydrocarbon peak) at 284.8 eV. Quantification (atomic percentage, At.%) was made using normalised peak area. The normalisation of the peak area and comparison of data from different elements were enabled by correction with empirically derived sensi- tivity factors, according to MultiPak library.

2.4. Evaluation of pore architecture of hydrogels

Hydrogel blocks were fixed overnight (ON) in 4% paraformalde- hyde at 4 °C and treated as previously reported (Yang, Jenkins, & Burg, 2007). Briefly, hydrogels were rinsed in 5% sucrose in phosphate buf- fered solution (PBS, pH 7.4) for 1 h, then cryoprotected by infiltrating them in PBS with ascending concentrations of sucrose (10%, 12.5%, 15%) at room temperature (~25 °C) every 30 min, then the hydrogels were stored in 20% sucrose in PBS ON at 4 °C. The 20% sucrose solution was discarded and the hydrogels were incubated for 1 h at room tem- perature with solutions in which the ratios of 20% sucrose in PBS and optimal cutting temperature medium (OCT®, Bio-Optica, Italy) were 2:1, 1:1 and 1:2 v/v. Hydrogels were stored in the last solution ON at 4 °C and then infiltrated with fresh OCT® at room temperature for 3 h to minimize shattering/cracking during the cryosectioning process. Thin cryosections (10 μm) were cut with a LeicaCM1950 cryostat, collected on Superfrost PlusTM microscope slides (ThermoFisher Scientific, Italy) and allowed to air dry.

Alternatively, freeze-dried hydrogels (drying procedure in 2.3) were rehydrated in ultrapure water for 24 h at 4 °C, and infiltrated for 2 h with a mixture of PBS/OCT® (1:1v/v), then ON in OCT® alone at 4 °C. Cryosections were obtained and collected as reported above. Sections were observed under transmitted light with a LeicaDM6000B micro- scope equipped with a 10X planar objective and imaged with a LeicaDFC310FX camera. The analysis of pore Feret's diameter and porosity

percentage was performed using ImageJ software. Scaffold porosity was calculated as the ratio between the voids and total surface and expressed as percentage. Calculation was done on six randomly- chosen images for each hydrogel type.

2.5. Release test

For release tests, three hydrogels of each type were incubated in 5 mL phosphate buffer (pH = 7.4) at 37 °C, an aliquot of 0.5 mL was collected from each specimen after 24, 48 and 72 h and an equal volume of fresh buffer was added. Released calcium and magnesium amounts were determined by the classic direct potentiometric method, exploiting ion selective electrodes (Lvova et al., 2018). To determine MGO release, a derivatisation reaction with o-phenylenediamine (OPD) was carried out (Adams et al., 2008). The reaction was performed at room temperature, in the dark. Samples were examined by an Agilent HPLC (1260Infinity, Agilent Technologies, US) equipped with a 20 µL Rheodyne injection loop, a Multiple Wavelength detector and a re- versed phase column (SynergiTMHydro-RP 4 µm 150 x 4.6 mm, Phenom- enex). An isocratic elution was performed at room temperature (flow rate 0.9 mL/min), using mobile phase (Water/ACN 75/25). The column effluent was constantly monitored at 263 nm and the OPD derivative of MGO was eluted after 3.50 min A linear response was observed for the standard curve (R2 = 0.995). Each analysis was performed in triplicate and results were reported as mean ± standard deviation.

2.6. Mechanical characterisation

Mechanical properties under compression of the hydrogels (cy- linder-shaped samples 1.6cm diameter and 2cm height) were eval- uated using a mechanical testing machine (EZ-SX, Shimadzu, Japan). Five specimens for each composition were tested at room temperature (21 °C). The crosshead speed was set at 1mm·min−1 and the load was applied while the specimen was compressed until break (~35-40% of original height). Young's compressive moduli (E) were calculated as the slope of the initial linear portion of the stress–strain curve (0–15%). Furthermore, compression tests of

rehydrated freeze-dried hydrogels were performed after immersion in PBS for 1 h. The resulting Young's compression modulus was calculated following the same procedure reported above. Then, to evaluate stress-relaxation properties, the hy- drogels were deformed with impermeable plates to a compressive strain of 10%, with a deformation rate of 50mm·min−1 to approximate an instantaneous deformation. Within 10% compression, the stresses versus strain relations of the gels were almost linear. Subsequently, the strain was held constant for 900 s, while the load was recorded as a function of time. The obtained data were analysed using MATLAB R2015a software (Bonifacio et al., 2017). In particular, fitting a third order exponential decay (Eq. 1) to the relaxation curves, three relaxation times were acquired. The increase in stress during straining was not included when fitting the relaxation curves. $\sigma t = A1 \cdot e^{-t/\tau 1} + A2 \cdot e^{-t/\tau 2} + A3 \cdot e^{-t/\tau 3} + y0$ (1) where σt is the total stress, while A1, A2 and A3 are the amplitudes corresponding to the three different relaxation times $\tau 1$, $\tau 2$ and $\tau 3$. Finally, to evaluate the gels viscosity, a first order exponential decay (Eq. 2) was fitted through the relaxation curves of every measurement. $\sigma t = A \cdot e^{-t/\tau} + y0$ (2) where σt is the total stress, while A is the amplitude corresponding to the relaxation time τ.

Moreover, the viscosity (η) was obtained multiplying the relaxation time τ by the linear equilibrium modulus Eeq, obtained fitting the initial linear part of the strain curve of the straining protocol and creating a linear fit.

2.7. Antibacterial activity evaluation

2.7.1. Bacterial growth conditions

Bacterial strains were clinical isolates tested for their multi-drug resistance (MDR) by the Novara Maggiore Hospital, Clinical Microbiology Unit. All the specimens were obtained after patient's in- formed consent and in full accordance with the Declaration of Helsinki. A single colony of S.aureus and S.epidermidis MDR strains from an ON culture onto differential and selective Mannitol Salt and Trypticase Soy (TSB) Agar plates was resuspended in 9 mL of Luria Bertani broth (LB) and incubated

at 37 °C for 18 h at 200 rpm. Then, cultures were diluted 1:10 in LB and incubated at 37 °C for 3 h (Lag phase) to achieve the logarithmic growth phase. Finally, a fresh culture was prepared for each experiment diluting bacteria until a concentration of 1 × 105cells/mL (o.d. at 600nm∼0.001) (Cochis et al., 2016).

2.7.2. Biofilm formation

To test antibacterial properties, hydrogel specimens were manu-

factured as 16 mm diameter, 3 mm thickness disks; these were gently handled by sterile surgical tweezers and placed onto the bottom of 24- well plates (without fixing the samples). Then, specimens were ster- ilised by UV-irradiation for 30 min/side. Sterile samples were covered with 1 mL of LB containing 1 × 105cells/mL. Samples were incubated for 90 min at 37 °C under agitation at 2 g (adhesion phase). Then, su- pernatants containing floating planktonic cells (separation phase) were removed and the specimens gently washed with 1mL of 1X PBS. Finally, each specimen was rinsed with 1 mL of fresh LB and incubated for 24, 48 and 72 h at 37 °C for biofilm culture.

2.7.3. Bacterial viability

A metabolic analysis, based on 2,3-Bis(2-methoxy-4-nitro-5-sulfo- phenyl)-2H-tetrazolium-5-carboxanilide assay (XTT) was performed to assess bacterial growth ability after 24, 48 and 72 h of direct contact with the hydrogels compared to polystyrene. Briefly, 100μL of XTT solution (0.3mg/mL in acetone containing 0.1M menadione) were added to each well and incubated at 37 °C for 5 h in the dark. Then, 50 μL were collected, centrifuged for 2 min at 480 g to remove debris and the o.d. was evaluated spectrophotometrically at 450 nm using a VICTOR Multilabel Plate Reader (Perkin Elmer, US). Bacteria viability onto polystyrene was considered as control.

2.8. In vitro biological tests

2.8.1. Eukaryotic cell culture conditions

Human mesenchymal stem cells (hMSCs) purchased from the American Type Culture Collection (adipose-derived, ATCC-PCS-500- 011) were cultured at 37 °C, 5% CO2 in basal medium intended as low- glucose Dulbecco's Modified Eagle Medium (DMEM) supplemented with 5% foetal bovine serum (FBS) and 5 ng/mL of human fibroblast growth factor-2 (hFGF-2). Cells were cultured until 70–80% confluency, detached by trypsin-EDTA and used between passages II-IV, to ensure undifferentiated state.

2.8.2. MSCs cytocompatibility

Hydrogels' cytocompatibility was investigated in vitro by direct and indirect assays to detect the possible presence of toxic compounds onto the hydrogel surfaces or released into the medium, respectively. For the direct assay, specimens were manufactured as 16 mm diameter, 3 mm thickness disks and placed into a 24-well plate by sterile tweezers for UV sterilization as prior described in 2.7.2. Then, 2 × 104 cells were seeded directly onto each sample surface in order to achieve a direct contact between cells and specimens' surface. Cells were diluted into 1 mL of basal medium (intended as low-glucose DMEM supplemented with 5% FBS and 5 ng/mL hFGF-2) and dropwise deposited onto spe- cimens' surface. For the indirect assay, 2 × 104 cells were seeded in the polystyrene bottom of a 24-wells plate and cultured in basal medium, with the test hydrogel suspended in a porous insert on the top of the same well to obtain a continuous release without a direct contact with cells. For both experiments, cell viability was evaluated after 1, 3, 5 and 7days by the XTT assay. At each time-point, medium was completely removed and replaced with 1 mL/specimen of XTT solution (3 mg/mL prepared in basal medium). The plates were incubated at 37 °C for 4 h in the dark, then 100 μL were collected from each test well and trans- ferred to a 96-well plate. The o.d. was evaluated spectrophotometrically at 450 nm by a VICTOR Multilabel Plate Reader (Perkin Elmer, US). Cells cultured onto polystyrene were considered as control (100% via-bility) to normalise the results (Cochis, Ferraris et al., 2017; Cochis, Grad et al., 2017).

2.8.3. Chondrogenesis

MSCs were directly seeded on hydrogels surface and cultured for 48 h in basal medium to allow adhesion and cell spread. Then, basal medium was replaced with chondrogenic medium (high glucose DMEM 4.5 g/L with 10% ITS + 1 Premix Tissue Culture Supplement, dex- amethasone 10−7M, ascorbate-2-phosphate 1 μM, 1% sodium pyruvate and TGF-β1 10 ng/mL) and cells were cultured for 21days. MSCs cul- tured onto polystyrene in the same conditions were used as positive control considering polystyrene as the gold standard material for stem cells cultivation and differentiation.

2.8.4. Chondrogenesis analysis

After 21days of culture, hMSCs chondrogenesis was evaluated by real-time Polymerase Chain Reaction (PCR) and histology. Cells were digested for 5 min with TRI reagent® and RNA was reverse transcribed with TaqMan reverse transcription kit using random hexamers. For real-time PCR, TaqMan Gene Expression Assays was used in a GeneAmp7500Real-Time PCR System (Applied Biosystems, USA). Data were normalised towards the endogenous control gene (18S rRNA) and reported as fold expression. Chondrogenic collagen-II (COLII), aggrecan (ACAN) and collagen-I (COLI) were analysed (Table 2). For histological

analysis, cells were fixed onto the specimens surfaces by a sucrose- formaldehyde solution (50:50, 10 min at RT) and stained with Safranin- O or Alcian blue (Cochis, Ferraris et al., 2017; Cochis, Grad et al., 2017).

2.9. Statistical analysis

Mechanical characterisation was studied on five replicates/sample type, while biological experiments were performed in triplicate. Statistical analysis of data was performed using the Statistical Package for Social Sciences (SPSSv.20.0, IBM, US). Data were compared by ANOVA, followed by Tukey's test. The significance level was set at $p < 0.05$. The Student's t-test for unpaired data was used for porosity measurements only.

3. Results and discussion

3.1 XPS characterisation

The elemental composition of the prepared hydrogels was studied by XPS analysis and reported in Fig.1A. As expected from GG and MH composition, the main elements detected were carbon and oxygen. Indeed, GG consists in a tetrasaccharide unit of glucose-glucuronic acid-glucose-rhamnose, repeated to form long linear chains [22]. Similarly, the content of total reducing sugars in MH (mainly glucose and fructose) was higher than 75% [23], while a wide range of phenolic and flavonoids compounds represented the minor MH constituents. Magnesium and calcium elements, deriving from the ionic crosslinking procedure, were also detected. Beyond the signals clearly ascribable to the polymeric matrix, the molecular spacer and crosslinking agents, the samples enriched with HNT additionally displayed silicon and aluminum signals in the characteristic 1:1 stoichiometry. The binding energies of silicon and aluminum signals, 102.8 and 74.2eV respectively, did not show any difference when HNT were included in all the hydrogel matrices. This finding suggested no hydrogen bonds formation between HNT and the organic network, differently from what observed in a previous work [13]. An accurate curve fitting of the C1s spectra (Fig.1B) revealed the overlapping of GG and MH contributions, making impossible an unequivocal interpretation. On the other hand, considering the binding energies of carboxylic acid groups, it was evident that, in the case of GG-MH-HNT Mg, this contribution fell at 289.0±0.1eV, whereas for the other samples it fell at 288.5±0.1eV. This result indicated a poor coordination between the cation and the gellan gum carboxylic acid groups for GG-MH-HNT Mg system. This lower interaction was in turn reflected both on swelling, cation release and on the mechanical performances of this hydrogel. Additional information relevant to these systems were obtained by FT-IR analysis, reported in the Supplementary material.

3.2 Evaluation of pore architecture of hydrogels

The ultrastructure of hydrogels was investigated on cryosections. Since the water content in the samples was high, we adapted a previously reported infiltration method to completely and gradually replace water with freezing medium before cryosectioning (Yang et al., 2007). Fig.2 showed micrographs of each hydrogel type before (A–D) and after freeze-drying (E–H). Void spaces are present in all hydrogels, likely representing cross-section areas of gel pores. HNT were easily detectable as darker particulate scattered in the hydrogel matrix (Fig.2B, D, F and H). The shape of the voids appeared more regular and round in Fig.2A–B compared with Fig.2C–D, regardless of the presence of HNT. Concerning the freeze-dried hydrogels, a different organization of voids, with larger voids surrounded by much smaller ones in all hydrogel matrices was observed (Fig. 2E–H). Fig. 2 I summarises the results of the analysis of mean Feret's diameter of the pore and the percentage of porosity. Statistical analysis, on Feret's diameter, found no significant difference in AvsB and CvsD but a significant difference in AvsC and BvsD (both $p < 0.0001$) with the voids of Mg2+-crosslinked hydrogels significantly smaller than Ca2+-crosslinked ones. Concerning freeze-dried hydrogels, there was no significant difference in GvsH. Statistically significant differences were obtained in EvsF ($p < 0.01$), EvsG and FvsH (both $p < 0.05$). The porosity of all samples (between 41 and 75%) may influence the mechanical behaviour of each hydrogel prepared. It has to be underlined that hydrated hydrogels did not show a porous internal structure (data not shown). As they cannot undergo the procedure of paraffin embedding, thus cryosectioning, preceded by the substitution of the water in the matrix, is the only method to cut and observe ultrathin slices. Freezing the samples at −20 °C before cutting and air drying of the sections may mimic a conventional procedure of freeze-drying. After conventional freeze-dehydration protocol, the hy- drogels were also studied. In both conditions, we observed a change of micro-architecture, shifting from a homogeneous

to a porous structure with pore diameter depending both on the drying protocol and the crosslinker used. This observation is fundamental as it suggests that, playing on different parameters (e.g. freeze-frying, crosslinker), a wide range of GG hydrogels suitable for different needs of regenerative medicine could be obtained. In all cases, the pore size and distribution are optimal for chondrocyte differentiation and cartilage regeneration.

Upper panels (A–D) refer to hydrated gels with different composi- tion. Lower panels (E–H) refer to freeze-dried hydrogels with the same composition. Magnification bars = 100 μm. (I) reports a detailed mea- surement of hydrogels pores.

In particular, the GG-MH-HNT Mg hydrogel showed a mean pore diameter (257 ± 48 μm) and porosity percentage (75%), that seems to better approach the required standard of an optimal scaffold for carti- lage regeneration (Tanaka et al., 2010).

3.3 Release test

Cationic release was studied in the early stages of conditioning in PBS (24, 48 and 72 h) (Fig. 3A–B). For calcium release, no significant differences were observed between GGeMH Ca and GG-MH-HNT Ca at each time-point (Fig. 3A). Conversely, the presence of HNT delayed magnesium ions release (*$p < 0.05$) (Fig. 3B), which might be ex- plained by the formation of transient bonds, encouraged by the higher mobility of Mg^{2+}, compared to Ca^{2+}, in the polymeric network.

This hypothesis is also supported by mechanical test (Section 3.4). Furthermore, the release of MGO from hydrogels was also evaluated by HPLC analysis, since in literature this molecule seems to have a re- markable influence on MH antibacterial performances (Stephens et al., 2010). The results of MGO release are shown in Fig. 3C. After 24 h of incubation, no significant differences were observed between the four crosslinked hydrogel types and the two non-crosslinked hydrogels. However, after 48 and 72 h, the amount of MGO released from non- crosslinked samples was remarkably higher than

that of the other hy- drogel types (*p < 0.05). Therefore, it could be hypothesised that Ca2+ and Mg2+ could play a pivotal role hindering MGO release. Conversely, HNT presence did not alter MGO release.

3.4 Mechanical characterisation

The mechanical properties of all the hydrogels were evaluated by static compression tests. As an example, Fig. 4A shows the stress-strain curve obtained compressing a GG-MH-HNT Mg sample at a strain of 0–35%. For each sample, compression Young's modulus (E) was cal- culated from the relevant stress-strain curves (Fig. 4C). Interestingly, all the samples showed high values of E (> 100 kPa) compared with other natural hydrogels for soft tissue and/or cartilage regeneration (Peak, Wilker, & Schmidt, 2013). Only HNT-reinforced gels showed a dramatic increase of E value compared with the non-reinforced samples. More- over, in this study, the compressive moduli of the prepared hydrogels were also higher (∼25-30%) than those of similar systems recently described (Bonifacio et al., 2017).

Thus, it could be hypothesised that MH, herein exploited for the first time as molecular spacer for hydrogel manufacturing, played a key role in the enhancement of the compressive moduli of the prepared systems. Furthermore, MH presence made the hydrogels more flexible and easy to handle. Concerning the impact of HNT addition on mechanical fea- tures, the inorganic filler did not significantly change the compressive moduli of the gels crosslinked with Ca2+ (GGeMH Ca 116 ± 5kPa vs GG-MH-HNT Ca 108 ± 10kPa). On the other hand, HNT presence dramatically improved the stiffness of Mg2+-crosslinked samples (102 ± 9kPa for GGeMH Mg vs 143 ± 8kPa for GG-MH-HNT Mg). This mechanical reinforcement could be attributed to the different ge- lification mechanisms introduced by Mg2+ and Ca2+ ions. In this re- spect, Donati and co-workers reported that Mg2+ act as diffusively bound ions rather than strongly site-bounded ions such as Ca2+ (Donati, Asaro, & Paoletti, 2009). This behaviour may allow a different mobility of the nanofillers in the

polymeric network. Therefore, in Mg2+-crosslinked hydrogels, HNT may orient and align under com- pression stress, establishing temporary bonds between polymer chains (without the formation of permanent hydrogen bonds, as revealed by XPS analysis), thereby creating a local region of enhanced strength. Conversely, in presence of Ca2+, HNT may become less mobile, pre- venting the occurrence of the energy dissipation mechanism hypothe- sised for Mg2+ (Shah, Maiti, Jiang, Batt, & Giannelis, 2005). Further- more, as described in Section 3.2, Mg2+-crosslinked hydrogels were characterised by a lower volumetric porosity than Ca2+-crosslinked ones. As largely described in literature, the porosity is inversely pro- portional to scaffolds compression moduli. Therefore, both parameters should be carefully considered in in vivo cell enrichments because, when the mechanical strength is sufficient to maintain the pore structure upon implantation, the pore volume determines the number of re- cruited cells (Kim, Li, Sands, & Mooney, 2014). Finally, the hydrogels mechanical properties were evaluated after rehydration of freeze-dried samples in PBS for 1 h. A non-statistically significant difference in the calculated moduli (compared with the values of the hydrated one) was observed (ranging from 12 to 15%), that indicates a high mechanical stability and consistency of the hydrogels. In addition to static com- pression tests, hydrogels viscoelasticity behaviour was studied by re- laxation experiments, in which the load decreased at fixed strain in response with time. It is noteworthy to compare the stress-relaxation behaviour of the prepared hydrogels with that of native tissues, since it affects loads transfer, as well as nutrients diffusion (Marijnissen et al., 2002). Fig. 4B shows the typical stress relaxation curve obtained after 900 s, reporting the relaxation times and viscosity values. A similar response was observed for all the samples: a fast decrease in stress for few seconds after the step strain, followed by a slow relaxation time. Wagenseil, Wakatsuki, Okamoto, Zahalak, and Elson, (2003) proposed the generalised Maxwell model, consisting in three relaxation times ($\tau1$ = 1–10 s, $\tau2$ = 10–100 s and $\tau3$ > 1000s) for modelling soft biolo- gical tissues to evaluate their viscoelastic behaviour. The calculated relaxation times ($\tau1$ 7–9 s, $\tau2$ 70–80 s and $\tau3$ 480–650 s)

were similar to the values reported in literature for polymeric gels (Wagenseil, et al., 2003). These relaxation times are related with the calculated

3.5 Antibacterial activity

Most of the studies on innovative biomaterials for cartilage repair lack of antibacterial active compounds, likely because arthroscopy-related infections are nowadays considered as very low risk episodes, affecting only 0.09 to 0.4% of patients undergoing surgery [40]. However, it must be considered that infections can determine septic arthritis, leading to potentially devastating post-operative complications [41]. Several case reports showed that the most commonly identified pathogens were *Staphylococci* strains [42]. Therefore, the prepared hydrogels were tested against clinical isolates of *S. aureus* (coagulase positive) and *S. epidermidis* (coagulase negative), as representative pathogens responsible for joint arthroscopy infections. To this respect, one of the strengths of this work is to exploit MH not only as innovative molecular spacer, but also as antibacterial agent. MH contains a large amount of MGO, which is considered among the most effective natural antibacterial compounds, due to its non-peroxide ac- tivity (Adams et al., 2008). MH contains 38–725mg/kg of MGO (Karygianni et al., 2016) while ordinary honey only 1.6–135 mg/kg. To give an example of MGO effectiveness, a minimum inhibitory con- centration for S. aureus was observed at 1.1mM of MGO (Mavric, Wittmann, Barth, & Henle, 2008). Considering these assumptions, the tested hydrogels were infected with S. aureus and S. epidermidis for 24, 48 and 72 h, to verify changes in bacterial viability (Section 2.7.3). Overall, the tested hydrogels were significantly effective in reducing S. aureus biofilm viability at each time-point in comparison with poly- styrene control (Fig. 5A, *$p < 0.05$). Particularly, GG-MH Mg samples resulted effective regardless of the presence of HNT, at each tested time- point. Conversely, the introduction of HNT significantly enhanced the antibacterial activity of Ca-crosslinked specimens (Fig. 5A, §$p < 0.05$). Furthermore, all hydrogel types reduced S. aureus viability more than 60% compared to control and

GG-MH-HNT Ca gels determined a via- bility reduction of more than 90% after 72 h. Concerning S. epidermidis, all tested hydrogels significantly reduced bacterial viability compared to controls at each time-point (Fig. 5B *$p < 0.05$), with the only ex- ception of GG-MH Mg after 24 h (likely due to the high standard de- viation). As observed for S. aureus, HNT increased the antibacterial activity of Ca-crosslinked hydrogels. However, for S. epidermidis, sig- nificant differences were noticed only after 24 h ($p < 0.05$,§). In agreement with the results obtained with S. aureus, bacterial viability was overall reduced more than 60% after 72 h. The raise of the anti- bacterial effect during the 24–72 h observation time (Fig. 5) was in line with Ca(II) and Mg(II) increased cumulative release from the analysed hydrogels as depicted in Fig. 3A-B.

To this regard, as evidenced by Xie and Yang (2016), although both the two alkaline-earth metal Ca(II) and Mg(II) ions are fundamental for many living organisms, they can also increase the antimicrobial activity of MH/GG composite hydrogels. Indeed, they are also necessary to se- lectively destabilize and destroy cytoplasmic membranes of MDR or wt S. aureus strains. This membrane-destabilization event likely occurs through their binding to cardiolipin, S. aureus' major lipid component also present in S. epidermidis (Luo, Javed, & Deneer, 2018) thus con- verting to negative its originally zero-intrinsic curvature.

3.6 Preliminary biocompatibility evaluations

3.6.1 Cytotoxicity

GG has been already described as a cytocompatible material for different purposes and in combination with other molecules (Koivisto et al., 2017), besides MH has been widely used in medicine. Moreover, according to the present literature, the free amount of the Ca2+ (Bronner, 2001) and Mg2+ (Romani, 2011) ions detected in the release test were not sufficiently large to determine significant variations in cells homeostasis. However, at the best of our knowledge, this

is the first time that GG is combined with MH and HNT at the same time. Therefore, considering that these composite materials are aimed for tissue engineering, their cytocompatibility was firstly evaluated to- wards hMSCs, normally recruited after tissue damage. During the direct assay, hMSCs viability was evaluated after 1, 3, 5 and 7 days of culture onto the hydrogels surfaces (Fig. 6C).

Overall, each hydrogel type allowed cell growth, as a general in- crease in o.d. was detected for all samples over time. No significant differences in terms of viability of cells cultured on the four hydrogel types were observed, with values always higher than 80%. Thus, be- yond their antibacterial effectiveness, the prepared hydrogels are sui- table to host hMSCs colonization, as other hydrogels proposed for cartilage repair (e.g. fibrin glue (Deponti et al., 2013), hyaluronic acid (Ha, Park, Chung, & Park, 2015) and methylcellulose (Cochis, Ferraris et al., 2017; Cochis, Grad et al., 2017). Furthermore, the indirect assay aimed at the study of the potential biomaterial toxicity, overcoming the effect due to the lack of adhesive signals, which is common on poly- saccharide-based hydrogels (Cochis, Ferraris et al., 2017; Cochis, Grad et al., 2017). None of the hydrogel types negatively affected hMSCs viability, which was not significantly different between all samples and controls at each time-point (Fig. 6D, $p > 0.05$). Moreover, the viability of cells cultured on the gels was always higher than 90% compared to controls. These findings are very encouraging, as the investigated sys- tems were effective in killing bacteria, but not toxic towards hMSCs.

3.7 Chondrogenesis evaluation

3.7.1 Gene expression

After the validation of the in vitro cytocompatibility, chondrogenesis

experiments were performed to test the hydrogels ability to support chondro-like matrix formation for further cartilage regeneration. All the produced materials were investigated in order to verify whether single ions or nanotubes-enriched composites could have represented an in- terference element during chondrogenesis in comparison with the same proceeding performed using the gold-

standard polystyrene surface. Real-time PCR results are reported in Fig. 7A–D. Chondrogenic genes COLII and ACAN were successfully expressed (Fig. 7A-B) and no sig- nificant differences were observed between samples and control in terms of fold expression ($p > 0.05$). The low expression of the osteo- genic COLI gene (Fig. 7B) confirmed that the cells correctly differ- entiated towards a cartilage-like matrix, as indicated by the positive COLII:COLI ratio (Fig. 7D).

This is an important confirmation of the cartilage-like matrix for- mation, since it is normally composed of 90% collagen-II and 10% other collagens (I-IV-V-VI-IX), that are very useful to stabilise the collagen-II fibril network (Fox, Bedi, & Rodeo, 2009). Moreover, according to real- time PCR results, cells seeded on hydrogels surfaces were positive for both Safranin-O and Alcian blue (Fig. 7E), confirming a massive pre- sence of GAGs and proteoglycans in the secreted extracellular matrix (Cochis, Ferraris et al., 2017; Cochis, Grad et al., 2017).

4. Conclusions and future perspectives

This work confirmed the interesting features of the prepared Manuka honey-gellan gum hydrogels: 1) intrinsic antibacterial activity, evaluated against two MDR Staphylococci strains 2) suitable mechanical properties, with compressive moduli (from 116 up to 143 kPa) even better than those of other natural hydrogels (from 10 to 60 kPa) already described in literature (Palumbo et al., 2015; Song et al., 2015). Therefore, the composite hydrogels herein described, combining for the first time Manuka honey and gellan gum, provide useful mechanical and antibacterial features for cartilage repair. Moreover, no cytotoxic effect of the hydrogels was observed when human mesenchymal stem cells were seeded on the gel surfaces. In addition, after 21days of cul- ture, chondrogenic differentiation occurred on hydrogels without dif- ferences with the control substrate. Interestingly, all the gels showed a microscopic porous internal architecture upon drying, thus paving the way for future studies in which cells will be allowed to colonise the inside of the hydrogels by fluidic

stimulation. Overall, the satisfying mechanical and biological data encourage a deeper investigation of the developed hydrogels, that have the potential to become implantable tools for cartilage repair.

Acknowledgements

This work was supported by Università degli Studi di Bari. Dr P. Gentile and Dr. A.M. Ferreira are members of the UK EPSRC Centre for Innovative Manufacturing of Medical Devices (MeDe Innovation, EPSRC grant EP/K029592/1). The authors would like to thank Mr. Stefano Sportelli, who kindly performed the methylglyoxal measure- ments, Dr. Stefano Andreoni (Novara Maggiore Hospital), who provided the MDR clinical isolates, Dr. Diletta Francesca Squarzanti who contributed to microbiological test.

References

Adams, C. J., Boult, C. H., Deadman, B. J., Farr, J. M., Grainger, M. N. C., Manley-Harris, M., et al. (2008). Isolation by HPLC and characterisation of the bioactive fraction of New Zealand manuka (Leptospermum scoparium) honey. Carbohydrate Research, 343, 651–659.

Anjum, S. (2016). Development of antimicrobial and scar preventive chitosan hydrogel wound dressings. International Journal of Pharmaceutics, 508(1–2), 92–101.

Bacelar, A. H., Silva-Correia, J., Oliveira, J. M., & Reis, R. L. (2016). Recent progress in gellan gum hydrogels provided by functionalization strategies. Journal of Materials Chemistry B, 4(37), 6164–6174.

Balato, G., Di Donato, S. L., Ascione, T., D'Addona, A., Smeraglia, F., Di Vico, G., et al. (2017). Knee septic arthritis after arthroscopy: Incidence, risk factors, functional outcome, and infection eradication rate. Joints, 5(02), 107–113.

Bert, J. M., Giannini, D., & Nace, L. (2007). Antibiotic prophylaxis for arthroscopy of the knee: Is it necessary? Arthroscopy, 23(1), 4–6.

Bonifacio, M. A., Gentile, P., Ferreira, A. M., Cometa, S., & De Giglio, E. (2017). Insight into halloysite nanotubes-loaded gellan gum hydrogels for soft tissue engineering applications. Carbohydrate Polymers, 163, 280–291.

Bronner, F. (2001). Extracellular and intracellular regulation of calcium homeostasis. The Scientific World Journal, 1, 919–925.

Caló, E., & Khutoryanskiy, V. V. (2015). Biomedical applications of hydrogels: A review of patents and commercial products. European Polymer Journal, 65, 252–267.

Carter, D. A., Blair, S. E., Cokcetin, N. N., Bouzo, D., Brooks, P., Schothauer, R., et al. (2016). Therapeutic Manuka honey: No longer so alternative. Frontiers in Microbiology, 7, 569.

Cochis, A., Azzimonti, B., Della Valle, C., De Giglio, E., Bloise, N., Visai, L., et al. (2016). The effect of silver or gallium doped titanium against the multidrug resistant aci- netobacter baumannii. Biomaterials, 80, 80–95.

Cochis, A., Ferraris, S., Sorrentino, R., Azzimonti, B., Novara, C., Geobaldo, F., et al. (2017). Silver-doped keratin nanofibers preserve a titanium surface from biofilm contamination and favor soft-tissue healing. Journal of Materials Chemistry B, 5(42), 8366–8377.

Cochis, A., Grad, S., Stoddart, M. J., Farè, S., Altomare, L., Azzimonti, B., et al. (2017). Bioreactor mechanically guided 3D mesenchymal stem cell chondrogenesis using a biocompatible novel thermo-reversible methylcellulose-based hydrogel. Scientific Reports, 7, 45018.

Deponti, D., Giancamillo, A. D., Gervaso, F., Domenicucci, M., Domeneghini, C., Sannino, A., et al. (2013). Collagen scaffold for cartilage tissue engineering: The benefit of fibrin glue and the proper culture time in an infant cartilage model. Tissue Engineering Part A, 20(5–6), 1113–1126.

Donati, I., Asaro, F., & Paoletti, S. (2009). Experimental evidence of counterion affinity in alginates: The case of nongelling ion Mg2+. The Journal of Physical Chemistry B, 113, 12877–12886.

Fox, S. A. J., Bedi, A., & Rodeo, S. A. (2009). The basic science of articular cartilage: Structure, composition, and function. Sports Health, 1(6), 461–468.

Ha, C. W., Park, Y. B., Chung, J. Y., & Park, Y. G. (2015). Cartilage repair using com- posites of human umbilical cord blood-derived mesenchymal stem cells and hya- luronic acid hydrogel in a minipig model. Stem Cells Translational Medicine, 4(9), 1044–1051.

Kaklamani, G., Cheneler, D., Grover, L. M., Adams, M. J., & Bowen, J. (2014). Mechanical properties of alginate hydrogels manufactured using external gelation. Journal of the Mechanical Behavior of Biomedical Materials, 36, 135–142.

Karygianni, L., Al-Ahmad, A., Argyropoulou, A., Hellwig, E., Anderson, A. C., & Skaltsounis, A. L. (2016). Natural antimicrobials and oral microorganisms: A sys- tematic review on herbal interventions for the eradication of multispecies oral bio- films. Frontiers in Microbiology, 6, 1529.
Kim, J., Li, W. A., Sands, W., & Mooney, D. J. (2014). Effect of pore structure of mac- roporous poly(Lactide-co-Glycolide) scaffolds on the in vivo enrichment of dendritic cells. ACS Applied Materials & Interfaces, 6(11), 8505–8512.
Koivisto, J. T., Joki, J. E., Parraga, R., Pääkkönen, L., Ylä-Outinen, L., Salonen, I., et al. (2017). Bioamine-crosslinked gellan gum hydrogel for neural tissue engineering. Biomedical Materials, 12(2), 025014.
Leone, G., & Barbucci, R. (2009). Polysaccharide based hydrogels for biomedical appli- cations. In G. Leone, & R. Barbucci (Eds.). Hydrogels – biological properties and appli- cations (pp. 25–41). Milan: Springer.
Liu, S. Q., Yang, C., Huang, Y., Ding, X., Li, Y., Fan, W. M., et al. (2012). Antimicrobial and antifouling hydrogels formed in situ from polycarbonate and poly(ethylene glycol) via Michael addition. Advanced Materials, 24(48), 6484–6489.
Liu, M., Zeng, X., Ma, C., Yi, H., Ali, Z., Mou, X., et al. (2017). Injectable hydrogels for cartilage and bone tissue engineering. Bone Research, 5(17014), 1–20.
Luo, Y., Javed, M. A., & Deneer, H. (2018). Comparative study on nutrient depletion- induced lipidome adaptations in Staphylococcus haemolyticus and Staphylococcus epidermidis. Scientific Reports, 8(2356), 1–10.
Lvova, L., Gonçalves, C. G., Di Natale, C., Legin, A., Kirsanov, D., & Paolesse, R. (2018). Recent advances in magnesium assessment: From single selective sensors to multi- sensory approach. Talanta, 179, 430–441.
Marijnissen, W. J., van Osch, G. I., Aigner, J., van der Veen, S. W., Hollander, A. P., Verwoerd-Verhoef, H. L., et al. (2002). Alginate as a chondrocyte-delivery substance in combination with a non-woven scaffold for cartilage tissue engineering. Biomaterials, 23(6), 1511–1517.
Mavric, E., Wittmann, S., Barth, G., & Henle, T. (2008). Identification and quantification of methylglyoxal as the dominant antibacterial constituent of Manuka (Leptospermum scoparium) honeys from New Zealand. Molecular Nutrition & Food Research, 52(4), 483–489.
Mouser, V. H., Melchels, F. P., Visser, J., Dhert, W. J., Gawlitta, D., & Malda, J. (2016). Yield stress determines bioprintability of hydrogels based on gelatin-methacryloyl and gellan gum for cartilage bioprinting. Biofabrication, 8(3), 1–13.
Nguyen, Q. T., Hwang, Y., Chen, A. C., Varghese, S., & Sah, R. L. (2012). Cartilage-like mechanical properties of poly (ethylene glycol)-diacrylate hydrogels. Biomaterials, 33(28), 6682–6690.
Palumbo, F. S., Fiorica, C., Di Stefano, M., Pitarresi, G., Gulino, A., Agnello, S., et al. (2015). In situ forming hydrogels of hyaluronic acid and inulin derivatives for car- tilage regeneration. Carbohydrate Polymers, 122, 408–416.
Peak, C. W., Wilker, J. J., & Schmidt, G. (2013). A review on tough and sticky hydrogels. Colloid and Polymer Science, 291(9), 2031–2047.
Romani, A. M. (2011). Cellular magnesium homeostasis. Archives of Biochemistry and Biophysics, 512(1), 1–23.
Sasikala, L., & Durai, B. (2015). Development and evaluation of chitosan honey hydrogel sheets as wound dressing. International Journal of Pharma and Bio Sciences, 6(1), 26–37.
Shah, D., Maiti, P., Jiang, D. D., Batt, C. A., & Giannelis, E. P. (2005). Effect of nano- particle mobility on toughness of polymer nanocomposites. Advanced Materials, 17, 525–528.
Song, K., Li, L., Li, W., Zhu, Y., Jiao, Z., Lim, M., et al. (2015). Three-dimensional dynamic fabrication of engineered cartilage based on chitosan/gelatin hybrid hydrogel scaf- fold in a spinner flask with a special designed steel frame. Materials Science and Engineering: C, 55, 384–392.

Speer, S. L., Schreyack, G. E., & Bowlin, G. L. (2015). Manuka honey: A tissue engineering essential ingredient. Journal of Tissue Science & Engineering, 6(2), 1–3.
Stephens, J. M., Schlothauer, R. C., Morris, B. D., Yang, D., Fearnley, L., Greenwood, D. R., et al. (2010). Phenolic compounds and methylglyoxal in some New Zealand manuka and kanuka honeys. Food Chemistry, 120, 78–86.
Stutz, G., Kuster, M. S., Kleinstück, F., & Gächter, A. (2000). Arthroscopic management of septic arthritis: Stages of infection and results. Knee Surgery, Sports Traumatology, Arthroscopy, 8(5), 270–274.
Tanaka, Y., Yamaoka, H., Nishizawa, S., Nagata, S., Ogasawara, T., Asawa, Y., et al. (2010). The optimization of porous polymeric scaffolds for chondrocyte/atelo- collagen based tissue-engineered cartilage. Biomaterials, 31(16), 4506–4516.
Visweswara Rao, P., Thevan Krishnan, K., Salleh, N., & Hua Gan, S. (2016). Biological and therapeutic effects of honey produced by honey bees and stingless bees: A com- parative review. Revista Brasileira de Farmacognosia, 26, 657–664.
Wagenseil, J. E., Wakatsuki, T., Okamoto, R. J., Zahalak, G. I., & Elson, E. L. (2003). One-dimensional viscoelastic behavior of fibroblast populated collagen matrices. Journal of Biomechanical Engineering, 125, 719–725.
Wang, F., Wen, Y., & Bai, T. (2016). The composite hydrogels of polyvinyl alcohol–gellan gum-Ca2+ with improved network structure and mechanical property. Materials Science and Engineering: C, 69, 268–275.
Wyatt, R. W., Maletis, G. B., Lyon, L. L., Schwalbe, J., & Avins, A. L. (2017). Efficacy of prophylactic antibiotics in simple knee arthroscopy. Arthroscopy, 33(1), 157–162.
Xie, Y., & Yang, L. (2016). Calcium and magnesium ions are membrane-active against stationary-phase staphylococcus aureus with high specificity. Scientific Reports, 6(20628), 1–8.
Yang, C., Jenkins, L., & Burg, K. J. L. (2007). Adapted cryosectioning method for hy- drogels used in regenerative medicine. Journal of Histotechnology, 30(3), 185–191. Yang, J., Zhang, Y. S., Yue, K., & Khademhosseini, A. (2017). Cell-laden hydrogels for osteochondral and cartilage tissue engineering. Acta Biomaterialia, 57, 1–25. Zhang, X., Zhang, W., & Yang, M. (2017). Application of hydrogels in cartilage tissue engineering. Current Stem Cell Research & Therapy in press.
Zhu, J., & Marchant, R. E. (2011). Design properties of hydrogel tissue-engineering scaffolds. Expert Review of Medical Devices, 8(5), 607–626.

Table 1
Nomenclature and nominal composition of the prepared hydrogels. All the %w/v are expressed in respect to 100 mL of water.

Sample Code	GG content (%w/v)	MH content (%w/v)	HNT content (%w/v)
GG-MH	2	2	–
GG-MH Ca	2	2	–
GG-MH Mg	2	2	–
GG-MH-HNT	2	2	0.5
GG-MH-HNT Ca	2	2	0.5
GG-MH-HNT Mg	2	2	0.5

Table 2
Primers and Probes Summary.

Gene	Abbreviation	Forward (5'-3')	Reverse (5'-3')	Probe (5'FAM/3'TAMRA)
Collagen type-I	COL 1	CCC TGG AAA GAA TGG AGA TGA T	ACT GAA ACC TCT GTG TCC CTT CA	CGG GCA ATC CTC GAG CAC CCT
Collagen type-II	COL 2	GGC AAT AGC AGG TTC ACG TAC A	GAT AAC AGT CTT GCC CCA CTT ACC	CCT GAA GGA TGG CTG CAC GAA ACA TAC
Aggrecan	ACAN	AGT CCT CAA GCC TCC TGT ACT CA	CGG GAA GTG GCG GTA ACA	CCG GAA TGG AAA CGT GAA TCA GAA TCA ACT

Gene	Abbreviation	Applied Biosystems Serial number
ribosomal 18S	18S	4310893E

A

Atomic percentage (%) calculated by XPS analysis						
Sample Type	C1s	O1s	Al2p	Si2p	Ca2p	Mg2p
GG-MH Ca	63.7	36.0	-	-	0.3	-
GG-MH-HNT Ca	79.1	20.3	0.2	0.2	0.2	-
GG-MH Mg	67.8	31.9	-	-	-	0.3
GG-MH-HNT Mg	74.4	24.9	0.3	0.2	-	0.2

B

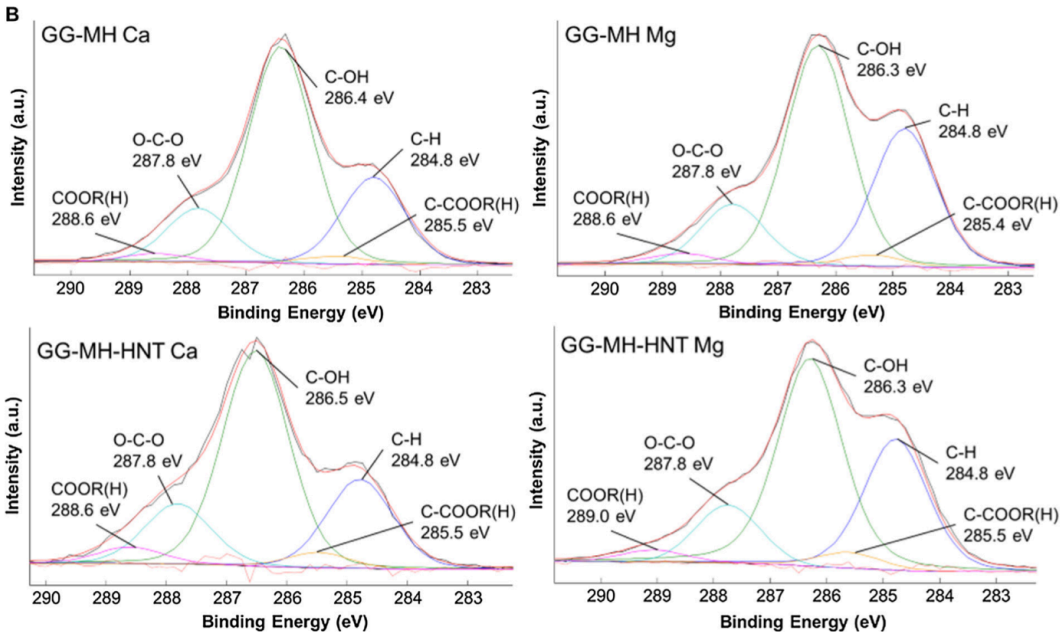

Fig. 1. XPS characterization of the prepared hydrogels. Relative atomic percentages calculated for each sample type (A). XPS curve fitting of high resolution C1s spectra of the relevant samples (B).

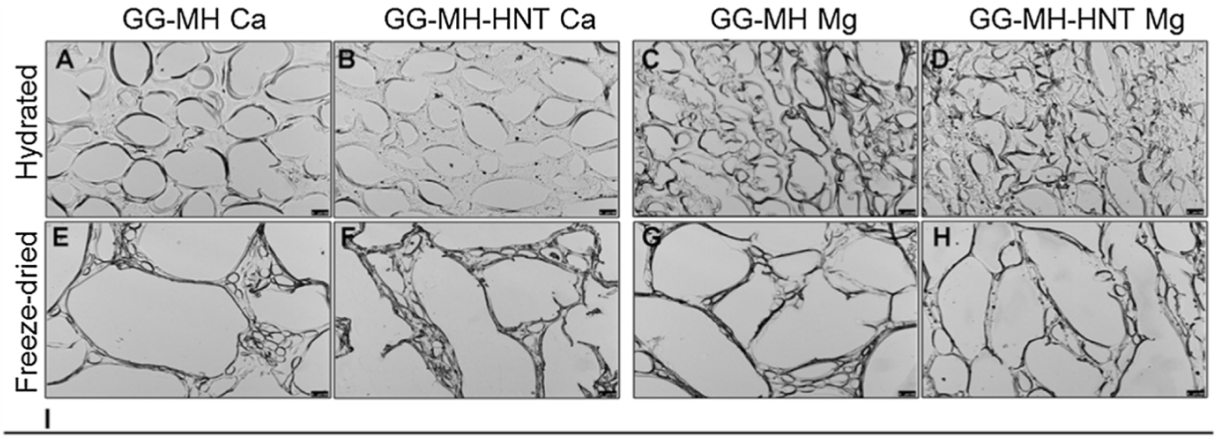

	A	B	C	D	E	F	G	H
Mean Feret's diameter (μm)±SEM	243±15	267±15	167±9	188±12	99±9	156±14	177±41	257±48
Statistical significance	A *vs* B n.s.	A *vs* C p<0.0001	B *vs* D p<0.0001	C *vs* D n.s.	E *vs* F P<0,001	E *vs* G p<0.05	F *vs* H p<0.05	G *vs* H n.s.
Porosity (%)	47	48	47	41	67	72	72	75

Fig. 2. Bright field micrographs of gellan gum scaffold hydrogels cryosections.

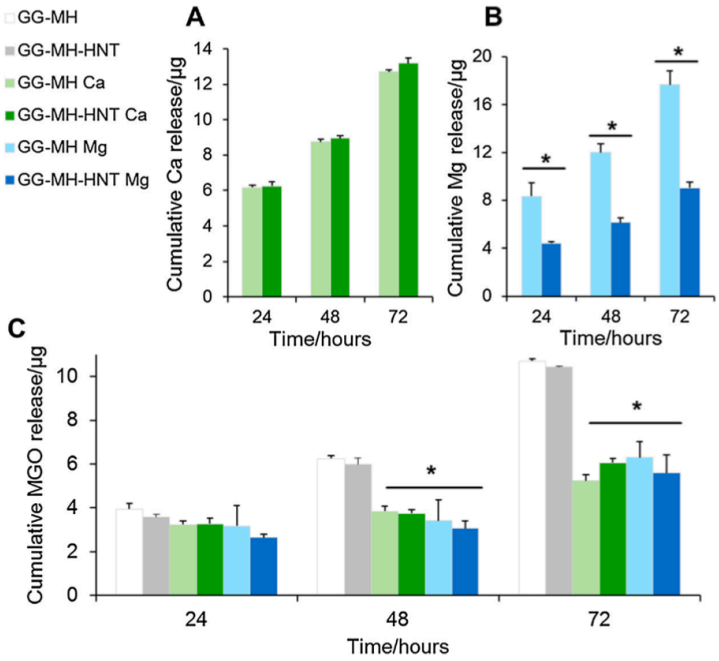

Fig. 3. Calcium (A) and magnesium (B) release from the prepared hydrogels, with or without HNT, after 24, 48 and 72 h. (C) Methylglyoxal release from the same samples. Statistically significant differences ($p < 0.05$) are indicated by the *.

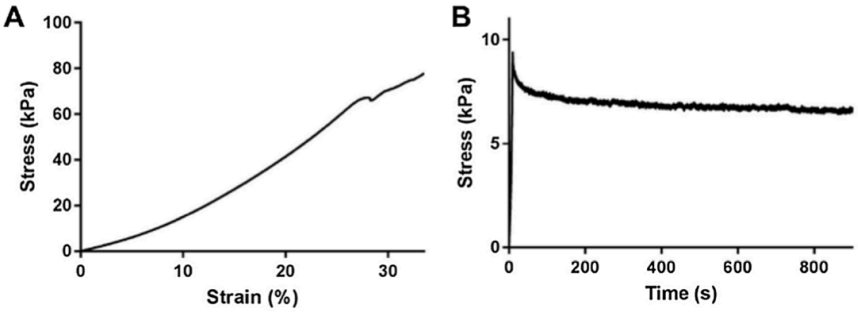

C

Composition	Young's compression modulus E, (kPa)	Relaxation time τ_1, (s)	τ_2, (s)	τ_3, (s)	Equilibrium modulus E_{eq}, (kPa)	Viscosity η, (MPa .s)
GG-MH Ca	116 ± 5	7.7 ± 0.8	72 ± 13	487 ± 42	72 ± 8	24 ± 3
GG-MH-HNT Ca	108 ±10	9.1 ± 1.2	86 ± 18	633 ± 31	88 ± 13	28 ± 3
GG-MH Mg	102 ± 9	8.1 ± 1.3	78 ± 12	512 ± 36	81 ± 12	25 ± 4
GG-MH-HNT Mg	143 ± 8	9.2 ± 0.9	87 ± 15	655 ± 49	98 ± 16	29 ± 5

Fig. 4. Mechanical characterization of the prepared hydrogels. (A) Stress-strain curve obtained by compression test. (B) stress-relaxation curve. (C) The table reports the Elastic moduli (E), relaxation times (τ_1, τ_2 and τ_3) and viscosities (η) relevant to each hydrogel type.

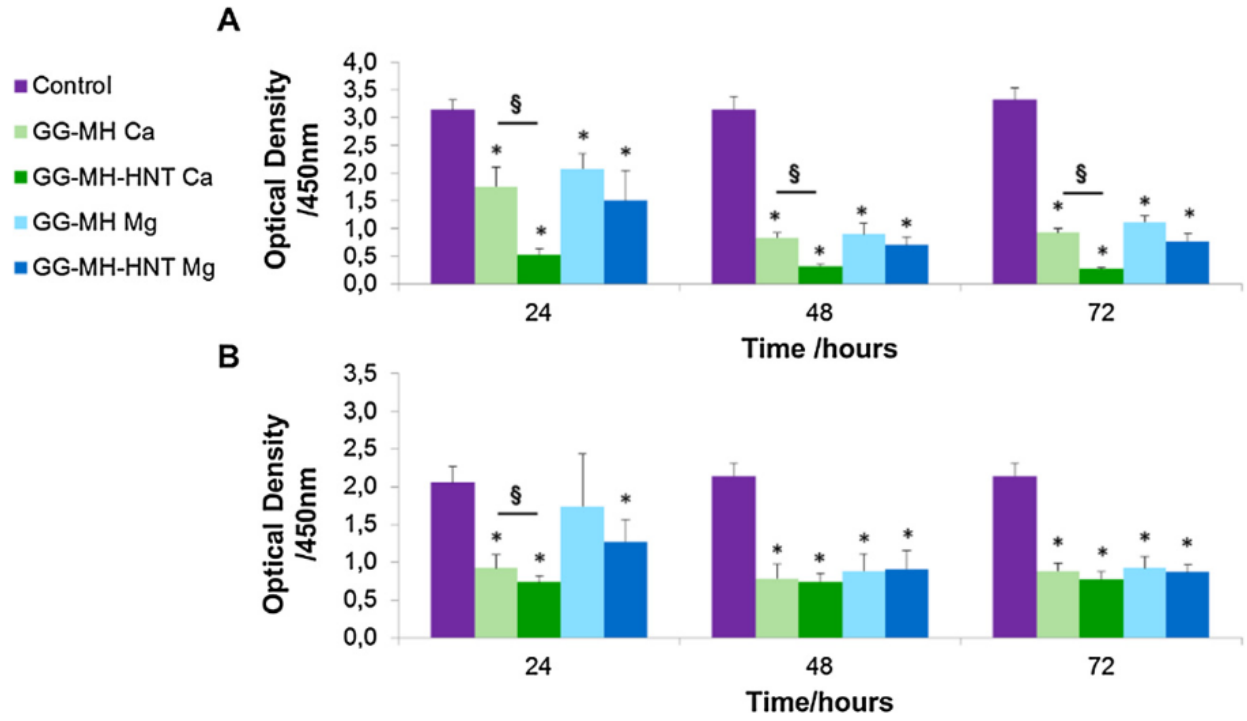

Fig. 5. Antibacterial activity of the hydrogels against *S. aureus* (A) and *S. epidermidis* (B). Biofilm viability after 24, 48 and 72 h. At each time point, all the tested specimens were effective in reducing biofilm viability in a significant manner in comparison with untreated controls ($p < 0.05$, indicated by the *). Bars represent means and standard deviations.

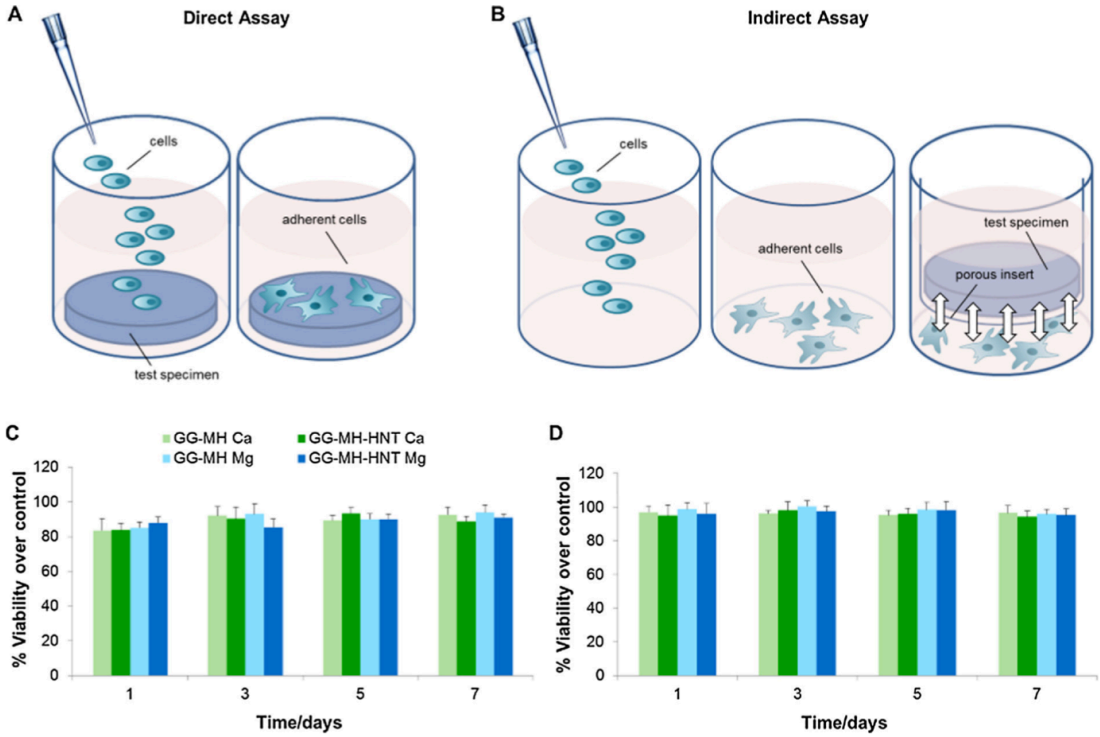

Fig. 6. Cytocompatibility evaluation. Direct cytocompatibility assay schematized in A. Stem cells viability was evaluated after 1, 3, 5 and 7 days after direct seeding onto specimens' surface (C). No significant differences were noticed between the four hydrogel types. Bars represent means and standard deviations. Indirect cytocompatibility assay (schematized in B). Stem cells viability at 1, 3, 5 and 7 days (D). No significant differences were noticed comparing all the hydrogels with untreated controls ($p > 0.05$). Normalized percentage viability was calculated considering untreated controls as 100%.

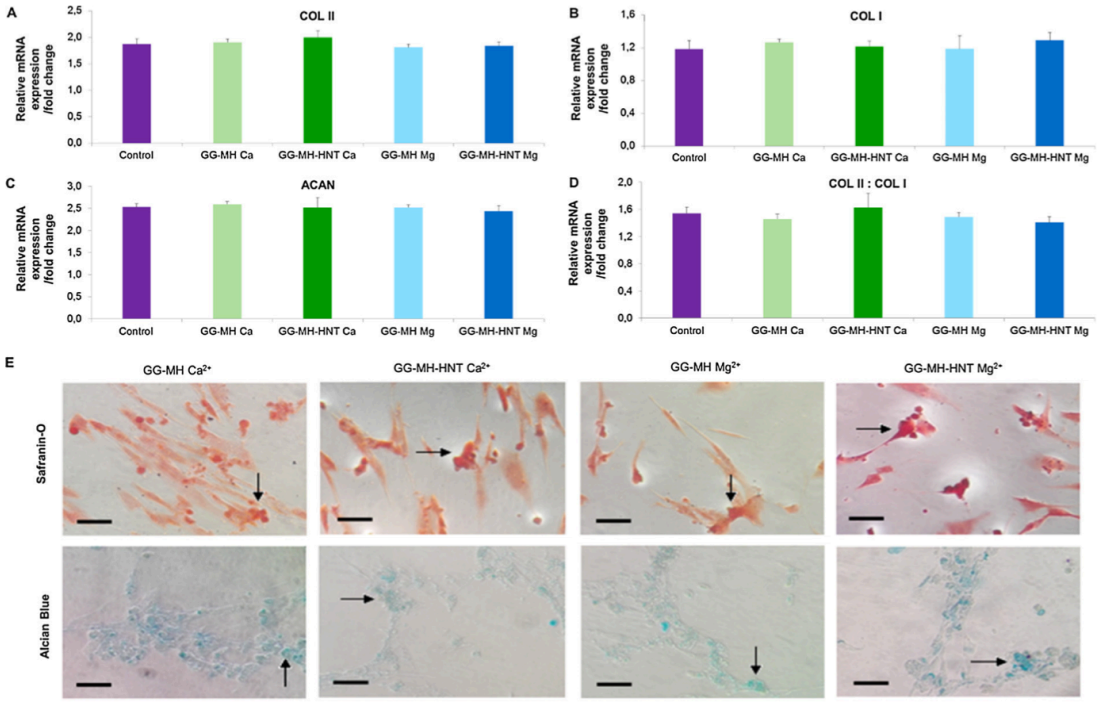

Fig. 7. Chondrogenesis evaluation. hMSCs cultivated onto specimens' surfaces successfully expressed chondrogenic genes collagen type II and aggrecan (A,C). No significant differences were detected between samples and control in terms of expression ratio ($p > 0.05$). Accordingly, cells expressed low levels of the osteogenic gene collagen type I (B) in comparison with collagen type II, as shown in (D). PCR results were confirmed by histology (E). Scale bars in (E): 50 μm.